Physics Letters B 763 (2016) 155–160

Contents lists available at ScienceDirect

Physics Letters B

www.elsevier.com/locate/physletb

Bounds on universal extra dimension from LHC run I and II data

Debajyoti Choudhury, Kirtiman Ghosh *

Department of Physics and Astrophysics, University of Delhi, Delhi 110007, India

ARTICLE INFO

Article history:
Received 16 June 2016
Received in revised form 18 September 2016
Accepted 6 October 2016
Available online 12 October 2016
Editor: A. Ringwald

ABSTRACT

We discuss the collider bounds on minimal Universal Extra Dimension (mUED) model from LHC Run-I and II data. The phenomenology of mUED is determined by only two parameters namely, the compactification scale (R^{-1}) of the extra dimension and cutoff scale (Λ) of the theory. The characteristic feature of mUED is the occurrence of nearly degenerate mass spectrum for the Kaluza–Klein (KK) particles and hence, soft leptons, soft jets at the collider experiments. The degree of degeneracy of KK-mass spectrum crucially depends on Λ. The strongest direct bound on R^{-1} (~ 950 GeV for large Λ) arises from a search for a pair of soft dimuons at the Large Hadron Collider (LHC) experiment with 8 TeV center-of-mass energy and 20 fb^{-1} integrated luminosity. However, for small Λ and hence, small splitting within the first KK-level, the bounds from the dimuon channel are rather weak. On the other hand, the discovery of 126 GeV Higgs boson demands small Λ to prevent the scalar potential form being unbounded from below. We discuss LHC monojet searches as a probe of low Λ region of mUED parameter space. We also compute bounds on the mUED parameter space from 13 TeV multijets results.

Theories with one or more extra space-like dimension(s) accessible to all or a few of the Standard Model (SM) fields are of interest for various reasons. For example, the ADD [1,2] (seemingly) and RS [3] models provide solutions to the long-standing naturalness/hierarchy problem by postulating the existence of compactified extra-dimension(s) accessible only to gravity with the SM fields being confined to a 3-brane embedded in the extra-dimensional bulk. On the other hand, there are a class of models wherein some or all of the SM fields can access the extended space–time manifold [2,4], whether fully or partially. Such extra-dimensional scenarios could lead to a new mechanism of supersymmetry breaking [2], relax the upper limit of the lightest supersymmetric neutral Higgs mass [5], give a different perspective to the issue of fermion mass hierarchy [6], interpret the Higgs as a quark composite leading to a electroweak symmetry breaking (EWSB) without a fundamental scalar or Yukawa interactions [7], lower the unification scale down to a few TeVs [8], provide a cosmologically viable candidate for dark matter [9,10], explain the long life time of proton [11], predict the number of fermion generations to be an integral multiple of three [12] and give rise to interesting signatures at collider experiments. As a result, search for the extra dimension(s) is one of the prime goals of the Large Hadron Collider (LHC) experiment [13,14]. Our concern here is a specific and particularly interesting framework, called the Universal Extra Dimension (UED) scenario.

The minimal version of UED (mUED) is characterized by a single flat extra dimension (y), compactified on an S^1/Z_2 orbifold with radius R, which is accessed by all the SM particles [4]. While a resolution of the hierarchy problem requires that $R^{-1} \sim \mathcal{O}(1\text{ TeV})$, it has long been argued that, in the absence of a dynamical stabilization of R^{-1} (or the cutoff), this is just a postponement of the explanation. However, recently, a mechanism for the stabilization of R^{-1} has been proposed in the context of higher-dimensional theories. The particle spectrum of mUED contains infinite towers of Kaluza–Klein (KK) modes (identified by an integer n, called the KK-number) for each of the SM fields with the zero modes being identified as the corresponding SM particles. The key feature of the UED Lagrangian is the conservation of the momentum along fifth direction. From a 4-dimensional perspective, this implies conservation of the KK-number. However, the additional Z_2 symmetry ($y \leftrightarrow -y$), which is required to obtain chiral structure of the SM fermions, breaks the translational invariance along the 5th dimension. As a result, KK-number conservation breaks down at loop-level, leaving behind only a conserved KK-parity, defined as $(-1)^n$. There are several interesting consequences of this discrete symmetry which, in turn, is an automatic outcome of the S^1/Z_2 orbifolding. KK-parity ensures the stability of the

* Corresponding author.
E-mail addresses: debajyoti.choudhury@gmail.com (D. Choudhury), kirti.gh@gmail.com (K. Ghosh).

http://dx.doi.org/10.1016/j.physletb.2016.10.010

Table 1
Benchmark points and mass spectrum of relevant level-1 particles. Total cross-sections (σ^{tot}) of KK-squarks/gluons pair production at the LHC with 8 and 13 TeV center-of-mass energy are also presented.

BPs	R^{-1} [GeV]	ΛR	m_{g_1} [GeV]	m_{Q_1} [GeV]	m_{q_1} [GeV]	m_{W_1/Z_1} [GeV]	m_{L_1} [GeV]	m_{B_1} [GeV]
BP1	920	3	1002	973	966	941	929	920
BP2	1100	3	1196	1163	1153	1125	1111	1099
BP3	1120	35	1414	1328	1300	1194	1157	1119

Total strong pair production cross-section [pb]			
$\sqrt{s}$	BP1	BP2	BP3
8 TeV	0.945	0.254	0.087
13 TeV	10.8	3.31	1.53

lightest KK-particle (LKP), allows only pair production of level-1 KK-particles at the collider, and prohibits KK-modes from affecting tree-level EW precision observables. And, although KK-modes do contribute to standard electroweak processes at higher orders, KK-parity ensures that, in a loop, they appear only in pairs resulting in a substantial suppression of such contributions.

Being a higher dimensional theory, mUED is nonrenormalizable and should be treated as an effective theory valid up to a cutoff scale Λ, expected to be somewhat larger than R^{-1}. With KK-parity ensuring that one-loop[1] mUED corrections to all electroweak observables are cutoff independent [15], the latter serve to constrain R^{-1}, almost independent of Λ. For example, low energy observables like muon $g-2$ [16], flavor changing neutral currents [17], $Z \to b\bar{b}$ decay [18], the ρ-parameter [19], $\bar{B} \to X_s\gamma$ [21] and other electroweak precision tests [20] put a lower bound of about 300–600 GeV on R^{-1}. This, along with the fact that the tree level mUED masses for level-n KK-excitations are given by $m_n^2 = m_0^2 + n^2 R^{-2}$ (m_0 being the mass associated with the corresponding SM field) implies that, within a given level, the excitations are quite degenerate. Quantum corrections partially lift this degeneracy [22] and, typically, B_1, the level-1 excitation of hypercharge gauge boson,[2] is the LKP, and, hence, stable. Being only weakly interacting, the B_1 turns out to be a good dark matter (DM) candidate [9]. Consistency with WMAP/PLANCK-measured [23] DM relic density data puts an upper bound of 1400 GeV on R^{-1}. Given this upper limit, it is extremely plausible that experiments at the LHC can either discover or rule out mUED. In this paper, we have discussed the impact of LHC Run I (center-of-mass energy $\sqrt{s} = 8$ TeV, integrated luminosity $\mathcal{L} = 20.3$ fb^{-1}) and Run II ($\sqrt{s} = 13$ TeV and $\mathcal{L} = 3.2$ fb^{-1}) results on mUED parameter space. In particular, we have obtained bounds on mUED parameter space from collider upper limits on the product of cross section, acceptance and efficiency ($\sigma \times A \times \epsilon$) in monojet [24,25] and multijets [26,27] plus missing energy ($\not{E}_T$) channels.

Given R^{-1} and, hence, the average KK-mass, the collider phenomenology is uniquely determined by the mass splittings, i.e., the quantum corrections. Apart from the usual radiative corrections that we expect in a Minkowski-space field theory, there are additional corrections accruing from the fact of the fifth direction being compactified on S_1/Z_2-orbifold. The correction terms can be finite (bulk correction) or logarithmically divergent (boundary correction). Bulk corrections arise only for the gauge boson KK-excitations due to the winding of the internal loop (lines) around the compactified direction [22]. The ubiquitous boundary corrections are just the counterterms of the total orbifold corrections, with the finite parts being completely unknown, dependent as they are on the details of the ultraviolet completion. Assuming that the boundary kinetic terms vanish at the cutoff scale Λ, the corrections from the boundary terms, at a renormalization scale μ would obviously be proportional to $\ln(\Lambda^2/\mu^2)$. Finite bulk corrections being subdominant, the cutoff scale plays the most crucial role in determining the mass-splitting and hence, the collider signatures of level-1 KK-particles. The perturbativity of the $U(1)$ gauge coupling requires that $\Lambda \lesssim 40R^{-1}$. It has been argued that a much stronger bound arises from the running of the Higgs-boson self-coupling and the stability of the electroweak vacuum [28,29]. However, note that such arguments were based only on the lowest-order calculations and the inclusion of higher-loops (which are poorly understood in this theory) can substantially change these results. Consequently, we will not impose the last-mentioned. In order to discuss the collider signatures and present the numerical results, we have chosen three benchmark points (BPs) listed in Table 1 along with the masses of relevant level-1 KK-particles. While the relatively small value of ΛR for BP1 and BP2 is reflected in the approximate degeneracy of level-1 KK-particles, a much larger value of the same for BP3 results in a wider splitting.

The level-1 KK-quarks (both the singlet q_1 and doublet Q_1) and gluons (g_1) are copiously produced in pairs at the LHC. These, subsequently, decay into SM particles and B_1 via cascades involving other level-1 KK-particles. As the spectra in Table 1 suggest, the g_1 can decay to both singlet (q_1) and doublet (Q_1) quarks with almost same branching ratios, with only a slight kinematic preference for the former. The singlet quark can decay only to B_1 and SM quark. On the other hand, the doublet quarks decay mostly to W_1 or Z_1. Hadronic decay modes of the W_1 being closed kinematically, it decays universally to all level-1 doublet lepton flavors (L_1 or ν_1), namely, $W_1 \to L_{i1}^{\pm}\nu_{i0}$ and $W_1 \to L_{i0}^{\pm}\nu_{i1}$ have equal branching ratios. Similarly, Z_1 can decay only to $L_1 l$ or $\nu_1\nu$ (with branching fractions being determined by the corresponding SM couplings). The KK leptons finally decay to the invisible B_1 and a ordinary (SM) lepton. Therefore, pair production of KK-quarks and/or gluon gives rise to jets + leptons + missing transverse energy $\not{E}_T$ signatures in the LHC experiments. Due to small SM background, leptonic final states [30–32] are considered to be the most promising channels for the discovery of UED at the LHC. However, due to the small splitting of level-1 KK-masses, in signal events, the jets/leptons as well as $\not{E}_T$ are, in general, soft thereby rendering the task a challenging one. Collider phenomenology of leptonic final states of mUED was discussed in details in Ref. [30] with a conclusion of opposite sign dilepton channel being the most promising for moderate $10R^{-1} < \Lambda < 40R^{-1}$. In order to enhance the signal to background ratio for soft signal leptons, the idea of imposing upper bounds on the lepton transverse momenta as well as on the invariant masses of lepton pairs was proposed in Ref. [32]. Recently, the ATLAS Collaboration, using 20.3 fb^{-1} integrated luminosity data for

[1] The observables start showing cutoff sensitivity of various degrees as one goes beyond one-loop or considers more than one extra dimension.

[2] The notation may seem confusing, but note that, owing to the large difference between the electroweak scale and R^{-1}, the analogues of the Weinberg angle are small for the KK-sectors.

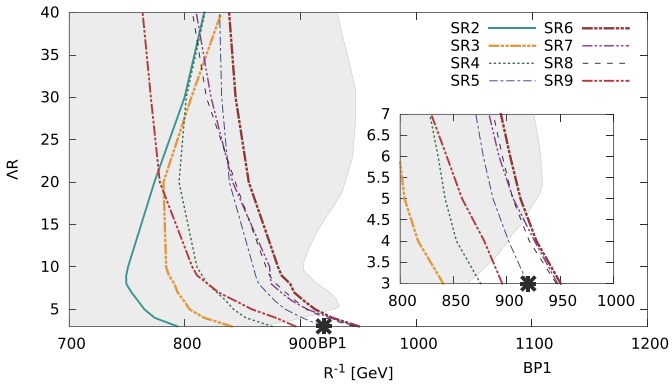

Fig. 1. 95% exclusion bounds on R^{-1}–ΛR plane from different SRs of ATLAS 8 TeV 20.3 fb^{-1} integrated luminosity monojet-like selection criteria. Low ΛR region is magnified in the inset. The shaded region corresponds to present ATLAS bound from dilepton plus $\not{E}_T$ search [14] at 8 TeV center-of-mass energy.

Table 2
Definitions of SRs for monojet-like selection used by ATLAS Collaboration in Ref. [25] along with 95% CL upper limits ($\langle\epsilon\sigma\rangle^{95}_{obs}$) on the product of cross section, acceptance and efficiency ($\sigma \times A \times \epsilon$). mUED cross-sections for the BPs are also presented.

Monojet-like selection criteria						
Preselection	SRs	$\not{E}_T >$ [GeV]	$\langle\epsilon\sigma\rangle^{95}_{obs}$ [fb]	σ(mUED) [fb] BP1	BP2	BP3
$\not{E}_T > 150$ GeV	SR1	150	726	70	15	28
At least one jet	SR2	200	194	52	11	21
With $p_T > 30$ GeV	SR3	250	90	37	7.6	13
$\lvert\eta\rvert < 4.5$	SR4	300	45	26	5.2	7.4
Lepton veto	SR5	350	21	19	3.8	3.6
Monojet-like sec.	SR6	400	12	**14**	2.8	1.6
$p_T^{j_1} > 120$ GeV	SR7	500	7.2	**7.6**	1.5	0.53
$\lvert\eta^{j_1}\rvert < 2.0$, $\frac{p_T^{j_1}}{\not{E}_T} > 0.5$	SR8	600	3.8	**4.0**	0.82	0.26
$\Delta\phi(\text{jet}, \vec{\not{E}}_T) > 1.0$	SR9	700	3.4	2.2	0.46	0.13

proton–proton collisions at $\sqrt{s} = 8$ TeV has performed a dedicated search for soft dimuons [14] (characterized by 6 GeV $< p_T^{\text{muon}} <$ 25 GeV and invariant mass cuts) specially designed to probe the mUED parameter space. In the absence of any significant excess of signal events over the SM backgrounds, they exclude, at 95% CL, the part of the parameter space, viz. the $(R^{-1}, \Lambda R)$ plane, depicted in gray in Fig. 1. Clearly, for large $\Lambda R \sim 35$, any R^{-1} below about 950 GeV is ruled out. However, for small $\Lambda R \sim 3$ (which is particularly motivated from the stability of scalar potential with a 126 GeV Higgs boson), the lower bound on R^{-1} is only about 860 GeV, a consequence of the very small splitting between level-1 KK-particles and, consequently, soft leptons evading the acceptance cuts. Hence, an alternative search strategy is called for.

A final state comprising a single jet, resulting primarily from initial state radiation, accompanied by a missing transverse energy could be a promising channel. Indeed, monojet plus $\not{E}_T$ is a very effective channel for theories with a quasi-degenerate spectrum, for example, in the search for third-generation squarks in compressed supersymmetry scenarios [33]. The spectrum of ISR jets depends on the scale and dynamics of the production process and is independent of the subsequent decay, including mass splittings. With the system of the pair of KK-particles (g_1g_1, g_1q_{i1}, $q_{i1}q_{j1}$, $q_{i1}\bar{q}_{j1}$) recoiling against a hard ISR jet, the final state comprises of a hard jet, substantial $\not{E}_T$ and some soft jets/leptons that may or may not be visible. Analyzing 20.3 fb^{-1} data from the 8 TeV run, the CMS [24] and ATLAS [25] Collaborations have used this channel to look for signatures of compressed SUSY, a generic DM candidate, large extra dimensions, very light gravitinos in a gauge-mediated supersymmetric model etc. In view of the consistency of experimental data and SM background predictions, model independent upper limits are set on the product of cross section, acceptance and efficiency ($\sigma \times A \times \epsilon$). Using the ATLAS results [25], we now perform an analogous exercise for mUED.

We generate the parton level events corresponding to pair production of KK-quarks/gluons using the mUED implementation [34] for the event generator PYTHIA [35]. We use the CTEQ6L1 [36] parton distributions with the factorization and renormalization scales kept fixed at the parton center-of-mass energy. ISR, decay of KK-quarks/gluons, showering and hadronization are also simulated with PYTHIA. For the reconstruction of physics objects (jets, leptons, $\not{E}_T$ etc.) we closely follow the prescription of Ref. [25] for ATLAS monojet + $\not{E}_T$ analysis. Jet candidates are reconstructed using FastJet [37] with the anti-k_T jet clustering algorithm [38] with a distance parameter of 0.4. Only jets with $p_T > 30$ GeV and $\lvert\eta\rvert < 4.5$ are considered for further analysis. Electron (muon) candidates are required to have $p_T > 7$ GeV and $\lvert\eta\rvert < 2.47(2.5)$. After identifying jets and leptons, overlaps between identified electrons and jets in the final state are resolved by discarding any jet candidate lying within a distance $\Delta R = \sqrt{\Delta\eta^2 + \Delta\phi^2} < 0.2$ of an electron candidate. Missing transverse momentum is reconstructed using all remaining visible entities, viz. jets, leptons and all calorimeter clusters not associated to such objects. After object reconstruction, only events with zero lepton, $\not{E}_T > 150$ GeV and at least one jet (satisfying the aforementioned preselection criteria) are selected for further analysis.

A monojet-like final state topology is demanding a leading jet with $p_T > 120$ GeV, $\lvert\eta\rvert < 2.0$ and $p_T/\not{E}_T > 0.5$. An additional requirement on the azimuthal separation $\Delta\phi(jet, \vec{\not{E}}_T) > 1.0$ between the direction of the missing transverse momentum and that of each of the selected jets is also imposed. After selecting events with monojet-like topology, different signal regions (SR1–SR9) are defined with progressively increasing thresholds for $\not{E}_T$. The ATLAS monojet-like selection criteria and signal regions are summarized in Table 2. For each of these signal regions, the good agreement between the numbers of events observed by the ATLAS detector and expected within the SM can be used to impose model-independent upper limits on the product $\sigma \times A \times \epsilon$, and these too are presented in Table 2. These should be compared with the monojet cross-sections for the mUED BPs which are presented in the last three columns of Table 2. Clearly, for BP1, the signal cross-sections exceed the ATLAS 95% CL upper limits ($\langle\epsilon\sigma\rangle^{95}_{obs}$) for each of SR6, SR7 and SR8. Thus, BP1, which had survived the dimuon search bounds ($R^{-1} = 860$ GeV for $\Lambda R \sim 3$), is squarely ruled out by the monojet analysis. While this may seem only a modest improvement, given that each of BP2 and BP3 survive, as we shall see below, this is crucial for a hole in the parameter space would have been left otherwise. Indeed, for low ΛR (preferred in the context of the stability of the Higgs potential), this constitutes the most promising channel. Our final exclusion limits in the R^{-1}–ΛR plane from different SRs of ATLAS $\sqrt{s} = 8$ TeV and $\mathcal{L} = 20.3$ fb^{-1} monojet + $\not{E}_T$ analysis are presented in Fig. 1.

The situation can be further improved if other channels are considered as well. A particularly useful one is that constituting multijets + $\not{E}_T$. Recently, both the ATLAS [26] and the CMS [27] Collaborations have communicated results for such an analysis for $\sqrt{s} = 13$ TeV, although for only a small data set (3.2 fb^{-1}). This, however, can be offset by an increased cross section. At the LHC, the dominant contribution to the pair production of level-1 KK-quarks/gluons arises from gluon–gluon or quark–gluon initial states. The gluon density increases by an order of magnitude as we go from 8 TeV to 13 TeV. Similarly, the presence of t-channel diagrams as well as the momentum-dependence of the vertices

Table 3
Definition of SRs for multijets plus $\not{E}_T$ analysis used by ATLAS Collaboration in Ref. [26] for 13 TeV center-of-mass energy and 3.2 inverse femtobarn integrated luminosity. $\Delta\phi(j, \vec{\not{E}}_T)$ is the azimuthal separations between $\vec{\not{E}}_T$ and the reconstructed jets. $m_{eff}(N_j)$ is defined to be the scalar sum of the transverse momenta of the leading N jets together with $\not{E}_T$. However, for $m_{eff}^{incl.}$, the sum goes over all jets with $p_T > 50$ GeV. Model independent 95% CL upper limits on multijets $\langle\epsilon\sigma\rangle_{\rm obs}^{95} = \sigma \times A \times \epsilon$ and mUED cross-sections for the BPs are also presented.

Cuts	Signal region						
	2jL	2jM	2jT	4jT	5j	6jM	6jT
$\not{E}_T >$ [GeV]	200	200	200	200	200	200	200
$p_T^{j_1} >$ [GeV]	200	300	200	200	200	200	200
$p_T^{j_2} >$ [GeV]	200	50	200	100	100	100	100
$p_T^{j_3} >$ [GeV]	–	–	–	100	100	100	100
$p_T^{j_4} >$ [GeV]	–	–	–	–	100	100	100
$p_T^{j_5} >$ [GeV]	–	–	–	–	–	100	100
$p_T^{j_6} >$ [GeV]	–	–	–	–	–	100	100
$\Delta\phi(j_{<3}, \vec{\not{E}}_T) >$	0.8	0.4	0.8	0.4	0.4	0.4	0.4
$\Delta\phi(j_{>3}, \vec{\not{E}}_T) >$	–	–	–	0.2	0.2	0.2	0.2
$\frac{\not{E}_T}{\sqrt{H_T}}$ [$\sqrt{\text{GeV}}$] >	15	15	20	–	–	–	–
Aplanarity >	–	–	–	0.04	0.04	0.04	0.04
$\frac{\not{E}_T}{m_{eff}^{N_j}} > [\sqrt{\text{GeV}}]$	–	–	–	0.2	0.25	0.25	0.2
$m_{eff}^{\text{incl.}} >$ [GeV]	1200	1600	2000	2200	1600	1600	2000
$\langle\epsilon\sigma\rangle_{\rm obs}^{95}$ [fb]	24	21	5.9	2.5	2.0	1.6	1.6
BP1	**36**	**66**	**11**	2.2	0.97	0.22	0.11
BP2	11	**24**	3.6	0.93	0.5	0.13	0.13
BP3	13	14	2.8	2.3	**2.2**	0.46	0.29

largely compensates for any suppression of the leading parton-level cross sections with an increase in the subprocess center of mass energy. For example, as Table 1 shows the total mUED production cross-section increases by a factor about 20 for KK-quark/gluon mass $\sim$ 1400 GeV. Therefore, it is instructive to study 13 TeV multijets + $\not{E}_T$ results in the context of mUED which we will discuss in the following.

The aforementioned ATLAS analysis [26] searched for events with 2–6 jets in association with a large $\not{E}_T$. Jet candidates are reconstructed using the anti-kt jet clustering algorithm with a distance parameter of 0.4, and only those with $p_T > 20$ GeV and $|\eta| < 2.8$ are retained. Electron (muon) candidates are required to have $p_T > 10$ GeV and $|\eta| < 2.47(2.5)$. Furthermore, a lepton needs to be isolated from a jet for the two entities to be reconstructed unambiguously. Consequently, any putative jet falling within an angular distance $\Delta R = 0.2$ of an electron is not reconstructed into a jet, leaving the constituents as unattached objects at that stage. Similarly, any electron falling within $\Delta R = 0.4$ of a surviving jet candidate is not considered as one, and its energy–momentum ascribed to the jet. The missing transverse momentum is reconstructed using all the remaining jets and leptons as well as all calorimeter clusters not associated to such objects. After the object reconstruction, events containing lepton(s) with $p_T > 10$ GeV are vetoed. Jets with $p_T > 50$ GeV are considered for further analysis.

The ATLAS Collaboration considers seven inclusive analysis channels, characterized by increasing jet multiplicity and different cuts to reduce the SM background. The effective mass, $m_{\rm eff}$, and $\not{E}_T$ turn out to be the most powerful discriminants between the multijets signal and SM backgrounds. These additional selection cuts are imposed on

- $\not{E}_T$
- $m_{\rm eff}^{\rm incl.}$ defined as the scalar sum of $\not{E}_T$ and the p_Ts of all jets with $p_T > 50$ GeV,
- $\not{E}_T/m_{\rm eff}^{N_j}$ (for events with *at least* N_j jets) where $m_{\rm eff}^{N_j} = \sum_{i=1}^{N_j} p_T^i(\text{jet}) + \not{E}_T$ with the sum extending over the leading N_j jets,
- $\not{E}_T/\sqrt{H_T}$ where $H_T = m_{\rm eff}^{\rm incl.} - \not{E}_T$,
- $\Delta\phi(\text{jet}, \vec{\not{E}}_T)$,
- the aplanarity variable A defined as $A = 3\lambda_3/2$, where λ_3 is the smallest eigenvalue of the normalized momentum tensor of the jets.

In Table 3, we list the cuts used by the ATLAS Collaboration to define the signal regions, and the corresponding model independent 95% CL upper limits on $\langle\epsilon\sigma\rangle_{\rm obs}^{95} = \sigma \times A \times \epsilon$.

For simulating the production of level-1 KK-quarks/gluons, their subsequent decays, ISR, showring and hadronization, we follow the same procedure as outlined before. The physics objects are reconstructed and events selected to mimic the ATLAS criteria described above. The signal cross-sections for the three BPs are presented in the last three rows of Table 3. BP1 and BP2 being characterized by low ΛR (and, hence, small splittings), typically give rise to low jet multiplicities. Whereas BP2 is seen to be ruled out by the '2jT' criteria, BP1 is ruled out by each of the three dijet SRs. On the other hand, BP3, owing to the larger R^{-1}, is associated with a smaller total cross section and easily evades the dijet constraints. However, owing to the much larger ΛR, the relative splittings are larger and a substantial fraction of events leads to multijet configurations. This, for example, allows us to rule it out using the '5j' SR.

In Fig. 2, we present the final exclusion bounds (drawn from the ATLAS analysis of the 3.2 fb^{-1} data collected in the 13 TeV run) in the mUED parameter space for each of the SRs listed in Table 3. The region in the $(R^{-1}, \Lambda R)$ to the right of a given curve is ruled out at 95% C.L. Note that for large ΛR ($\gtrsim 30$), the strongest bounds come from an analysis of final state with at least 5 jets and is about 1130 GeV. The sensitivity falls drastically for the inclusive six-jet final state. This can be understood by realizing that, at the parton level, the decay of the KK-particles would lead to at most four SM quarks/gluons (and, that too only for $g_1 g_1$ production). For low ΛR ($\lesssim 16$), on the other hand, the strongest bound ($R^{-1} \gtrsim 1110$ GeV) is achievable from the '2jM' signal region. It is worthwhile to note that the basic requirements (one jet with $p_T > 300$ GeV, another jet with $p_T > 50$ GeV and $\not{E}_T > 300$ GeV)

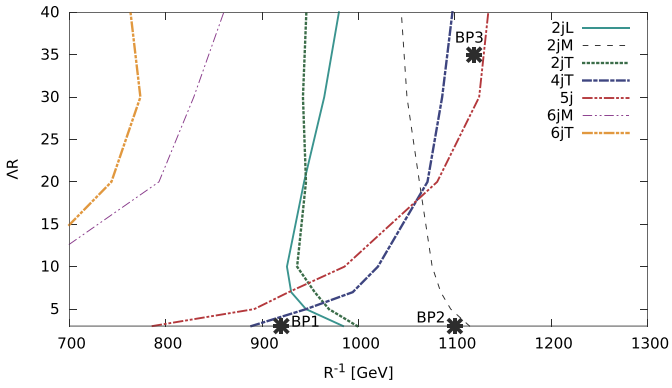

Fig. 2. 95% exclusion bounds on R^{-1}–ΛR plane from different SRs of ATLAS 13 TeV 3.2 fb^{-1} integrated luminosity multijets plus $\not{E}_T$ analysis.

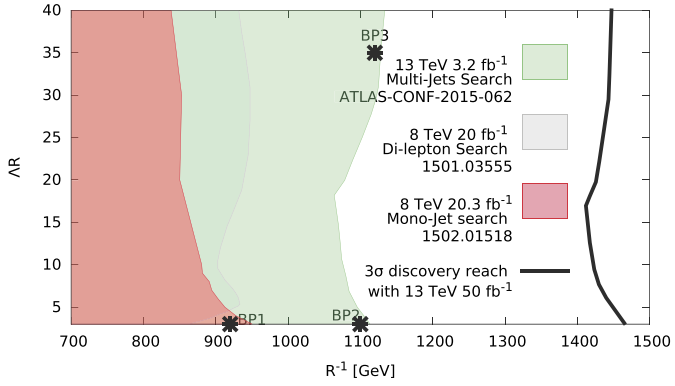

Fig. 3. Regions of R^{-1}–ΛR plane excluded from ATLAS Run I monojet and lepton [14] analysis as well as Run II 3.2 fb^{-1} multijets plus $\not{E}_T$ searches. The solid line corresponds to 3σ discovery reach for $\sqrt{s} = 13$ TeV and 50 fb^{-1} integrated luminosity with the multijets event selections described in Table 3.

for the '2jM' signal region are markedly similar to the monojet-like selection criteria used earlier. Hence, it comes as no surprise that this constitutes the most efficient strategy for low ΛR.

To summarize, we have computed constraints on the mUED parameter space using the ATLAS 8 TeV monojet results. While the dedicated ATLAS search strategy (involving soft dimuons) is a promising one for large ΛR, it is not very efficient for low ΛR, a region preferred by certain theoretical considerations, such as the stability of the Higgs potential. On the other hand, the monojet channel, being independent of the mass splitting (and, hence, ΛR) does not suffer from the drawbacks of the soft dimuon channel, and is seen to be much more sensitive (in this region) than the latter. This, clearly, calls for the inclusion of mUED as a candidate scenario for any future monojet study at ATLAS/CMS. We also examine the efficacy of the multijet ($+\not{E}_T$) signal in the context of mUED. Even with the small sample size analyzed by the ATLAS Collaboration, this is shown to lead to a much stronger exclusion of the mUED parameter space, as is depicted in Fig. 3, wherein the different shaded regions correspond to the individual exclusions allowed by different search strategies. The solid line in Fig. 3 corresponds to 3σ discovery reach for $\sqrt{s} = 13$ TeV and 50 fb^{-1} integrated luminosity with the multijets event selections described in Table 3. A casual perusal of Fig. 3 might suggest that the multijet channel is overwhelmingly superior. This should be treated with caution, though. For one, the particular sub-channel that is the most sensitive one for $\Lambda R \lesssim 16$ is the one that is remarkably close to the monojet algorithm, experimental results for which do not yet exist for the 13 TeV run. Similarly, the inclusion of multijet final state along with soft but isolated leptons (i.e., without the lepton veto being imposed as was done in the ATLAS analysis) is likely to lead to some improvement in the sensitivity.

Acknowledgements

DC acknowledges partial support from the European Union's Horizon 2020 research and innovation program under Marie Sklodowska-Curie Grant No. 674896, and the R&D grant of the University of Delhi. KG is supported by DST (India) under INSPIRE Faculty Award DST-INSPIRE-PH-117.

References

[1] N. Arkani-Hamed, S. Dimopoulous, G. Dvali, Phys. Lett. B 429 (1998) 263; I. Antoniadis, N. Arkani-Hamed, S. Dimopoulos, G.R. Dvali, Phys. Lett. B 436 (1998) 257.
[2] I. Antoniadis, Phys. Lett. B 246 (1990) 377.
[3] L. Randall, R. Sundrum, Phys. Rev. Lett. 83 (1999) 3370; L. Randall, R. Sundrum, Phys. Rev. Lett. 83 (1999) 4690.
[4] T. Appelquist, H.C. Cheng, B.A. Dobrescu, Phys. Rev. D 64 (2001) 035002; H.C. Cheng, K.T. Matchev, M. Schmaltz, Phys. Rev. D 66 (2002) 056006.
[5] G. Bhattacharyya, S.K. Majee, A. Raychaudhuri, Nucl. Phys. B 793 (2008) 114.
[6] N. Arkani-Hamed, M. Schmaltz, Phys. Rev. D 61 (2000) 033005.
[7] N. Arkani-Hamed, H.C. Cheng, B.A. Dobrescu, L.J. Hall, Phys. Rev. D 62 (2000) 096006.
[8] K. Dienes, E. Dudas, T. Gherghetta, Nucl. Phys. B 537 (1999) 47; K.R. Dienes, E. Dudas, T. Gherghetta, Phys. Lett. B 436 (1998) 55; For a parallel analysis based on a minimal length scenario, see S. Hossenfelder, Phys. Rev. D 70 (2004) 105003; G. Bhattacharyya, A. Datta, S.K. Majee, A. Raychaudhuri, Nucl. Phys. B 760 (2007) 117.
[9] G. Servant, T.M.P. Tait, Nucl. Phys. B 650 (2003) 391; H.C. Cheng, J.L. Feng, K.T. Matchev, Phys. Rev. Lett. 89 (2002) 211301; K. Kong, K.T. Matchev, J. High Energy Phys. 0601 (2006) 038; D. Hooper, S. Profumo, Phys. Rep. 453 (2007) 29.
[10] B.A. Dobrescu, D. Hooper, K. Kong, R. Mahbubani, J. Cosmol. Astropart. Phys. 0710 (2007) 012.
[11] T. Appelquist, B.A. Dobrescu, E. Ponton, H.U. Yee, Phys. Rev. Lett. 87 (2001) 181802.
[12] B.A. Dobrescu, E. Poppitz, Phys. Rev. Lett. 87 (2001) 031801.
[13] S. Chatrchyan, et al., CMS Collaboration, Phys. Rev. Lett. 108 (2012) 111801; S. Chatrchyan, et al., CMS Collaboration, J. High Energy Phys. 1105 (2011) 093; S. Chatrchyan, et al., CMS Collaboration, Phys. Rev. D 87 (11) (2013) 114015; V. Khachatryan, et al., CMS Collaboration, Eur. Phys. J. C 75 (5) (2015) 235; G. Aad, et al., ATLAS Collaboration, J. High Energy Phys. 1603 (2016) 026; G. Aad, et al., ATLAS Collaboration, Phys. Rev. D 92 (3) (2015) 032004; G. Aad, et al., ATLAS Collaboration, J. High Energy Phys. 1508 (2015) 148.
[14] G. Aad, et al., ATLAS Collaboration, J. High Energy Phys. 1504 (2015) 116; L. Morvaj, CERN-THESIS-2014-284, 2014.
[15] P. Dey, G. Bhattacharyya, Phys. Rev. D 70 (2004) 116012; P. Dey, G. Bhattacharyya, Phys. Rev. D 69 (2004) 076009.
[16] P. Nath, M. Yamaguchi, Phys. Rev. D 60 (1999) 116006; K. Agashe, N.G. Deshpande, G.H. Wu, Phys. Lett. B 511 (2001) 85.
[17] D. Chakraverty, K. Huitu, A. Kundu, Phys. Lett. B 558 (2003) 173, Nucl. Phys. B 660 (2003) 225; A.J. Buras, A. Poschenrieder, M. Spranger, A. Weiler, Nucl. Phys. B 678 (2004) 455; K. Agashe, N.G. Deshpande, G.H. Wu, Phys. Lett. B 514 (2001) 309.
[18] J.F. Oliver, J. Papavassiliou, A. Santamaria, Phys. Rev. D 67 (2003) 056002.
[19] T. Appelquist, H.U. Yee, Phys. Rev. D 67 (2003) 055002.
[20] T.G. Rizzo, J.D. Wells, Phys. Rev. D 61 (2000) 016007; A. Strumia, Phys. Lett. B 466 (1999) 107; C.D. Carone, Phys. Rev. D 61 (2000) 015008; I. Gogoladze, C. Macesanu, Phys. Rev. D 74 (2006) 093012.
[21] U. Haisch, A. Weiler, Phys. Rev. D 76 (2007) 034014.
[22] H.C. Cheng, K.T. Matchev, M. Schmaltz, Phys. Rev. D 66 (2002) 036005.
[23] E. Komatsu, et al., WMAP Collaboration, Astrophys. J. Suppl. Ser. 192 (2011) 18; P.A.R. Ade, et al., Planck Collaboration, arXiv:1502.01589 [astro-ph.CO].
[24] V. Khachatryan, et al., CMS Collaboration, Eur. Phys. J. C 75 (5) (2015) 235.
[25] G. Aad, et al., ATLAS Collaboration, Eur. Phys. J. C 75 (7) (2015) 299, Eur. Phys. J. C 75 (9) (2015) 408 (Erratum).
[26] The ATLAS Collaboration, ATLAS-CONF-2015-062.
[27] V. Khachatryan, et al., CMS Collaboration, Phys. Lett. B 758 (2016) 152–180, http://dx.doi.org/10.1016/j.physletb.2016.05.002.
[28] A. Datta, S. Raychaudhuri, Phys. Rev. D 87 (3) (2013) 035018.
[29] A. Datta, A. Patra, S. Raychaudhuri, Phys. Rev. D 89 (9) (2014) 093008.
[30] B. Bhattacherjee, K. Ghosh, Phys. Rev. D 83 (2011) 034003.

[31] G. Bhattacharyya, A. Datta, S.K. Majee, A. Raychaudhuri, Nucl. Phys. B 821 (2009) 48;
H. Murayama, M.M. Nojiri, K. Tobioka, Phys. Rev. D 84 (2011) 094015;
A. Belyaev, M. Brown, J. Moreno, C. Papineau, J. High Energy Phys. 1306 (2013) 080;
G. Servant, Mod. Phys. Lett. A 30 (15) (2015) 1540011;
K. Ghosh, J. High Energy Phys. 0904 (2009) 049;
K. Ghosh, S. Mukhopadhyay, B. Mukhopadhyaya, J. High Energy Phys. 1010 (2010) 096.
[32] D. Choudhury, A. Datta, K. Ghosh, J. High Energy Phys. 1008 (2010) 051.
[33] G. Aad, et al., ATLAS Collaboration, Phys. Rev. D 90 (5) (2014) 052008;
M. Aaboud, et al., ATLAS Collaboration, arXiv:1604.07773 [hep-ex].
[34] M. ElKacimi, D. Goujdami, H. Przysiezniak, P.Z. Skands, Comput. Phys. Commun. 181 (2010) 122.
[35] T. Sjostrandet, et al., J. High Energy Phys. 0605 (2006) 026.
[36] J. Pumplin, et al., J. High Energy Phys. 0207 (2002) 012.
[37] M. Cacciari, et al., Eur. Phys. J. C 72 (2012) 1896.
[38] M. Cacciari, G.P. Salam, G. Soyez, J. High Energy Phys. 0804 (2008) 063.